The Journal of Experimental Biology 205, 3271–3279 (2002)
Printed in Great Britain © The Company of Biologists Limited
JEB4412

Quantification of the wake of rainbow trout (*Oncorhynchus mykiss*) using three-dimensional stereoscopic digital particle image velocimetry

Jennifer C. Nauen and George V. Lauder*

Department of Organismic and Evolutionary Biology, Harvard University, Cambridge, MA 02138, USA

*Author for correspondence (e-mail: glauder@oeb.harvard.edu)

Accepted 7 August 2002

Summary

Although considerable progress has been made within the last decade in experimental hydrodynamic analyses of aquatic locomotion using two-dimensional digital particle image velocimetry (two-dimensional DPIV), data have been limited to simultaneous calculation of two out of the three flow velocity variables: downstream (*U*), vertical (*V*) and lateral (*W*). Here, we present the first biological application of stereo-DPIV, an engineering technique that allows simultaneous calculation of *U*, *V* and *W* velocity vectors. We quantified the wakes of rainbow trout (*Oncorhynchus mykiss*, 16.5–21.5 cm total body length, *BL*), swimming steadily in a recirculating flow tank at a slow cruising speed of 1.2 *BL* s^{-1}. These data extend the comparative basis of current hydromechanical data on the wakes of free-swimming fishes to the salmoniforms and are used to test current hypotheses of fin function by calculations of mechanical performance and Froude efficiency.

Stereo-DPIV wake images showed three-dimensional views of oscillating jet flows high in velocity relative to free-stream values. These jet flows are consistent with the central momentum jet flows through the cores of shed vortex rings that have been previously viewed for caudal fin swimmers using two-dimensional DPIV. The magnitude and direction of *U*, *V* and *W* flows in these jets were determined over a time series of 6–8 consecutive strokes by each of four fish.

Although the fish swam at the same relative speed, the absolute magnitudes of *U*, *V* and *W* were dependent on individual because of body size variation. Vertical flows were small in magnitude (<1 cm s^{-1}) and variable in direction, indicating limited and variable vertical force production during slow, steady, forward swimming. Thus, in contrast to previous data from sunfish (*Lepomis macrochirus*) and mackerel (*Scomber japonicus*), the trout homocercal caudal fin does not appear to generate consistent vertical forces during steady swimming. *U* flows were of the order of 3–6 cm s^{-1}; lateral flows were typically strongest, with *W* magnitudes of 4–6 cm s^{-1}. Such strong lateral flows have also been shown for more derived euteleosts with homocercal caudal fins.

The ratios of the magnitudes of wake flow, *U*/(*U*+*V*+*W*), which is a flow equivalent to mechanical performance, were also dependent on individual and ranged from 0.32 to 0.45, a range similar to the range of mechanical performance values previously determined using standard two-dimensional DPIV methods for caudal fin locomotion by more derived euteleosts. Strong lateral jet flow appears to be a general feature of caudal fin locomotion by teleosts and may reflect the nature of undulatory propulsion as a posteriorly propagated wave of bending. Froude efficiency (η_p) was independent of individual; mean η_p was 0.74, which is similar to previous findings for trout.

Movies available on-line

Key words: locomotion, swimming, rainbow trout, efficiency, stereoscopic digital particle image velocimetry, *Oncorhynchus mykiss*.

Introduction

Studies of locomotor hydrodynamics in fish have entered a new phase within the last decade with the application of the technique of digital particle image velocimetry (DPIV). DPIV allows quantitative visualization of flow fields created by freely moving fishes, which is an advantage over more qualitative approaches such as tracking streams of dye introduced into the flow and inference of flow patterns from kinematic data. DPIV involves visualizing flow by adding reflective, inert, near-neutrally buoyant particles to fluid and illuminating the particles in a planar section of flow using a laser light sheet. Flow-field characteristics including velocity and vorticity are calculated from successive images of particle movement captured at high frequency (Raffel et al., 1998). Wake momentum and force can be calculated from DPIV velocity vector fields (e.g. Drucker and Lauder, 1999, 2001a). DPIV has become a popular method for quantifying wakes produced by the caudal fin of fishes (Stamhuis and Videler, 1995; Müller et al., 1997; Hanke et al., 2000; Lauder, 2000; Liao and Lauder,

2000; Müller et al., 2000; Drucker and Lauder, 2001b; Nauen and Lauder, 2002).

To date all studies of aquatic locomotion using DPIV have used two-dimensional DPIV methods, in which flow is visualized separately in one plane, typically the parasagittal (*xy*) or frontal (*xz*) plane. A few studies have combined two-dimensional measurements of the three flow velocity variables, downstream (*U*), vertical (*V*) and lateral (*W*), calculated from separate kinematic events measured with different planar light sheet orientations to estimate the three-dimensional structure of wake flow patterns (e.g. Drucker and Lauder, 1999, 2000; Nauen and Lauder, 2002). Such three-dimensional reconstructions require study of a repetitive behavior that shows little kinematic variation among repetitions, such as pectoral fin locomotion by bluegill sunfish (*Lepomis macrochirus*) (Drucker and Lauder, 1999, 2000) and caudal fin locomotion by chub mackerel (*Scomber japonicus*) (Nauen and Lauder, 2002).

These limitations of two-dimensional analysis can be avoided by using three-dimensional stereoscopic DPIV, in which the use of two cameras with two different fields of view allows simultaneous visualization of all three velocity components using only a single light sheet orientation. While stereo-DPIV is well established in the engineering literature (Gaydon et al., 1997; Lawson and Wu, 1997; Willert, 1997; Westerweel and van Oord, 2000), this is the first application of this technique to the study of biologically generated flow patterns. Hence, the first goal of this study was to test the utility of stereo-DPIV to study wakes created by freely swimming fishes.

Our second goal was to examine the vortex wake of a salmoniform fish. This group represents a major phylogenetic grouping within ray-finned fishes for which few experimental hydrodynamic data are available, although this clade has been the subject of extensive previous research on locomotory performance. For example, the steady swimming kinematics (Stevens, 1979; Webb et al., 1984; Webb, 1988, 1993) and energetics (Webb, 1971a,b), myotomal slow muscle locomotory function (Hammond et al., 1998) and muscle power output (Coughlin, 2000) of *Oncorhynchus mykiss* have been examined previously, although the hydrodynamics of locomotion by *O. mykiss* remain unexplored except for the preliminary report of Blickhan et al. (1992).

Wake structure reveals important information about the timing, magnitude and direction of thrust production as well as potentially interesting data on the mechanisms of thrust production. On the basis of previous studies of trout steady swimming kinematics (Stevens, 1979; Webb et al., 1984; Webb, 1988, 1993) and wake structure (Blickhan et al., 1992), it is likely that trout wakes are composed of linked vortex rings with oscillating central jet flows that are high in lateral velocity (and are thus similar to the wakes of other body–caudal fin swimmers). The expectation that trout wakes would be composed of linked vortex-ring wakes such as those previously visualized using various two-dimensional techniques (Anderson, 1996; Müller et al., 1997; Videler et al., 1999; Hanke et al., 2000; Drucker and Lauder, 2001b; Nauen and Lauder, 2002) offered an advantage in using trout rather than a completely uncharacterized system as a test of the application of stereo-DPIV to aquatic locomotory systems.

The third goal of this study was to examine two specific features of the salmoniform vortex wake in the light of current data on the function of the homocercal caudal fin in teleost fishes (for a review, see Lauder, 2000). Previous studies of more derived clades (Gibb et al., 1999; Lauder, 2000; Nauen and Lauder, 2002) have suggested that the homocercal caudal fin, which is externally symmetrical in shape, can generate lift forces due to asymmetrical movements that direct flow dorsally or ventrally. We quantified wake flow patterns to determine whether the homocercal caudal fin of rainbow trout was directing flow dorsally or ventrally, and thus producing lift, during steady swimming. In addition, previous studies of more derived clades using two-dimensional DPIV have demonstrated that lateral flow velocities are typically higher than the downstream flow velocities, resulting in surprisingly low caudal fin mechanical performance ratios of approximately 0.35 (out of a possible maximum value of 1) for taxa as varied as bluegill sunfish *Lepomis macrochirus* (Drucker and Lauder, 2001b) and chub mackerel *Scomber japonicus* (Nauen and Lauder, 2002). We used the simultaneously measured magnitudes of *U*, *V* and *W* produced by *O. mykiss* during steady swimming to determine whether the ratio of downstream to total wake flow magnitude is similar to the previously reported caudal fin mechanical performance measurements for more derived species. Values of Froude propulsive efficiency, an index of overall locomotory efficiency, were also calculated from the velocity measurements for comparison both with values from other studies and with values of caudal fin mechanical performance.

Materials and methods

Animals

Rainbow trout, *Oncorhynchus mykiss* (Walbaum), were purchased from a local fish hatchery. The trout were fed commercial trout food and housed in 1200 l tanks at a water temperature of 15°C with a 12 h:12 h light:dark photoperiod. Four fish with a total body length (*BL*) range of 16.5–21.5 cm and a mean body length of 18.9±1.0 cm (mean ± S.E.M., *N*=4) were used.

Stereoscopic DPIV flow visualization

Experiments were conducted using a 600 l recirculating flow tank. The flow tank has a working area of 82 cm×28 cm×28 cm (length × width × height). Water temperature was 15±1°C. Flow speed in the tank was controlled using a variable-speed motor. Details of the flow tank and flow speed calibration have been presented previously (Jayne et al., 1996; Gibb et al., 1999). A flow tank was used to control the speed of the fish and to provide a relatively small field of view for the images (approximately 15 cm×7 cm, length × height) for a close view of the wake (see Figs 2, 3).

Fish swam at 1.2 $BL\,s^{-1}$, which matches the speed used for

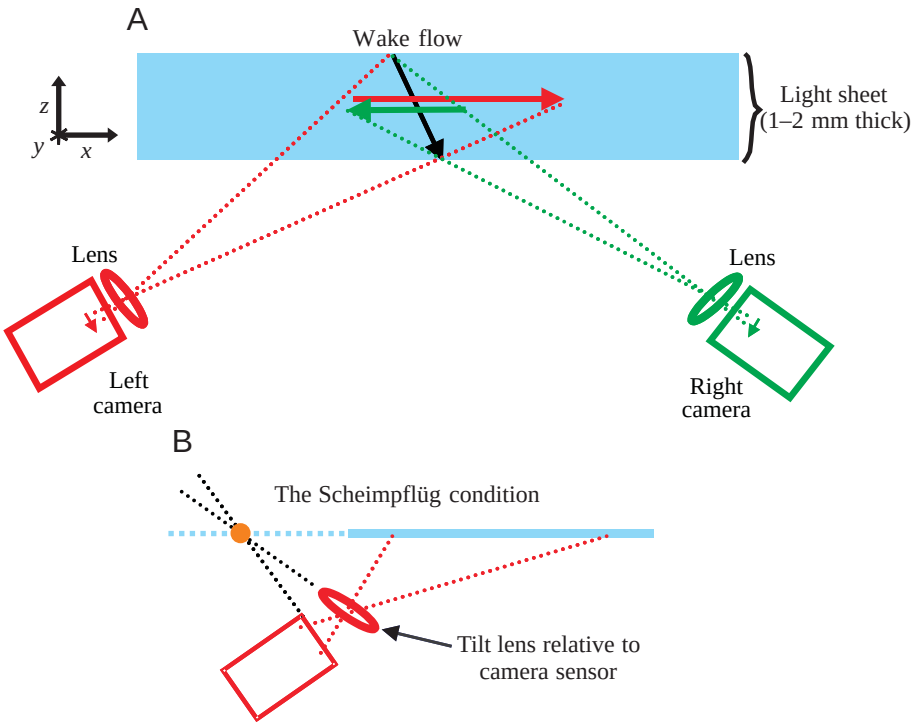

Fig. 1. Equipment configuration for stereo-DPIV flow visualization viewed from above (*xz* plane). The laser light sheet (shown in blue) is positioned in the center of the flow tank. Two cameras are placed at a wide angle relative to the laser light sheet (A). The thick black arrow (A) represents wake flow, which is shown with a relatively large lateral trajectory angle (i.e. high magnitude of *W*, which is flow in the *z* dimension) to illustrate differences between the field of view of the two cameras. The red and green dotted lines and arrows for the left and right cameras, respectively, represent the different fields of view of each camera and the resulting two-dimensional views of flow movement in opposite directions. Each camera's lens is tilted relative to the camera (B) in the Scheimpflüg configuration so that the light sheet plane, the image plane and the lens principal plane intersect at a common line (depicted here as an orange circle), and the plane of best focus is the light sheet plane. The Scheimpflüg configuration results in a clear and sharp image of particles illuminated by the light sheet, despite the large camera angles. See Materials and methods for more details.

several previous two-dimensional DPIV studies of caudal fin locomotion (Liao and Lauder, 2000; Drucker and Lauder, 2001b; Nauen and Lauder, 2002) and is close to speeds examined in other two-dimensional DPIV studies of caudal fin locomotion (Müller et al., 1997, 2001). The relatively low flow velocities also facilitated the calculation of out-of-plane particle movement (see below). Only video sequences during which the trout swam steadily and did not drift either vertically or laterally were analyzed. Steady swimming behavior was determined by visually evaluating the *xy* position of the dorsal and ventral tips of the caudal fin as it moved through the light sheet during each stroke. Error is estimated to be of the order of 2 mm, which is substantially less than 5% of the field of view of the cameras (15 cm×7 cm).

As in previous two-dimensional DPIV studies conducted in this laboratory (e.g. Drucker and Lauder, 2000; Lauder, 2000; Wilga and Lauder, 2000; Nauen and Lauder, 2001, 2002), flow was visualized by seeding the water with near-neutrally buoyant 12 μm diameter silver-coated glass beads (density 1.3 g cm^{-3}, Potters Industries, USA) that reflected light from an 8 W argon-ion laser (Fig. 1). The laser light sheet was approximately 2 mm×7 cm×15 cm (depth × height × width). It was positioned in the center of the working section of the flow tank, and oriented in the parasagittal (*xy*) plane. Data were collected when the fish was positioned so that the caudal fin beat through the light sheet in mid-stroke.

A key characteristic of the stereo-DPIV arrangement is the use of two cameras (Fig. 1) to view the light sheet. For two-dimensional measurements (see studies cited above), a single camera is positioned perpendicular to the light sheet. Stereo-DPIV measurements require two synchronized cameras both positioned at a wide angle to the light sheet (Fig. 1), so that each camera records a different, but overlapping, perspective of the flow. In the present study, two Redlake Motionscope model PCI 500 digital video cameras were used. Images of 480×420 pixels resolution were recorded at a frequency of 250 Hz.

A second novel characteristic of the stereo-DPIV arrangement is the camera lens position and orientation. Lenses are uncoupled from the body housing the camera sensor and tilted relative to the camera to achieve the Scheimpflüg stereoscopic configuration (Fig. 1B) in which the object plane (in this case, the light sheet), the image plane and the lens principal plane intersect in a common line. Tilting the lens of each camera relative to the camera's CCD sensor (using a custom-designed mounting bracket) makes the plane of best focus the plane of the light sheet, rather than the plane perpendicular to the camera's optical axis. This results in images that are bright and in good focus across the field of view for accurate vector calculations.

The camera arrangement and Scheimpflüg lens orientation introduce perspective distortion. For example, the cameras view a rectangular calibration grid illuminated by the light sheet as a trapezoid (Fig. 2A). This image distortion is corrected by recording simultaneous views of a three-dimensional calibration grid (Fig. 2A). Calibration marker points in a square grid with a fiducial mark at grid center (Fig. 2A) define the coordinate system and match calibration

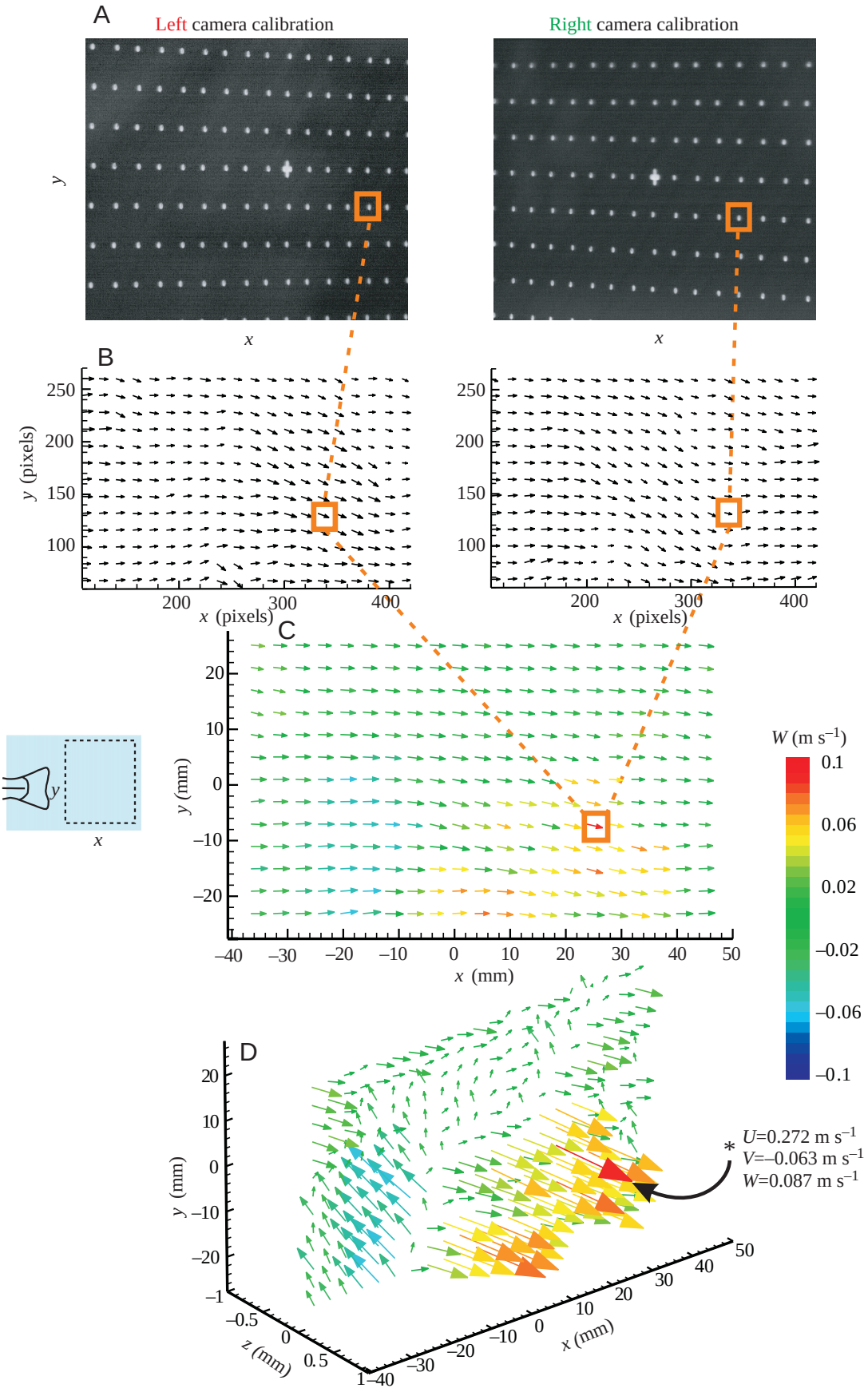
A
Left camera calibration
Right camera calibration
y
x
x
B
250
200
150
100
y (pixels)
200
300
400
x (pixels)
250
200
150
100
200
300
400
x (pixels)
C
y
x
20
10
0
–10
–20
y (mm)
–40
–30
–20
–10
0
10
20
30
40
50
x (mm)
W (m s–1)
0.1
0.06
0.02
–0.02
–0.06
–0.1
D
20
10
0
–10
–20
y (mm)
–1
–0.5
0
0.5
1
z (mm)
–40
–30
–20
–10
0
10
20
30
40
50
x (mm)
*
U=0.272 m s–1
V=–0.063 m s–1
W=0.087 m s–1

Fig. 2. A schematic view of stereo-DPIV image processing and calculation methods using data from a trout 21.5 cm in total body length (*BL*) swimming at 1.2 *BL* s^{-1} with a freestream velocity in the *x* direction, *U*, of 25.8 cm s^{-1}. Images of the three-dimensional calibration grid (A) recorded from the two cameras show distortion of the two-dimensional views caused by the camera arrangement and Scheimpflüg configuration (Fig. 1). The uniform, symmetrical calibration grid appears slanted, with a decreased vertical distance between rows on the inner sides of both images. Image alignment and distortion are corrected using polynomial equation mapping functions created using a least-squares method and the calibration grid points. Each of the two cameras (Fig. 1) collects two-dimensional images of the wake from which two-dimensional velocity vectors (dimensions scaled in pixels, B) are calculated. Note that freestream *U* has not been subtracted from these calculations; the high value of *U* results in a downstream trajectory for both sets of two-dimensional vectors (unlike the diagram in Fig. 1), and that vector density was decreased for viewing clarity. The orientation of the trout caudal fin relative to the light sheet is depicted as a small icon below B. The two-dimensional vectors are used to calculate three-dimensional flow fields (scaled in m s^{-1}; C,D). Vector color in C and D indicates the magnitude of *W* (the lateral or *z* velocity component); note that free-stream flow has not been subtracted. Orange boxes connected by broken lines represent the alignment between areas of the calibration images (A), two-dimensional velocity vectors calculated from DPIV images scaled with the calibration images (B) and the final three-dimensional velocity vectors (viewed in the parasagittal plane in C, and viewed in three dimensions in D by rotating the parasagittal plane counterclockwise). The vector calculated for the image area identified by the orange boxes in A, B and C is identified by a black arrow in D, with the magnitude of its *U*, *V* and *W* components given. Rotating C counterclockwise shows strong lateral jet flow (emphasized here by the small scale of the *z* axis for ease of viewing) that alternates to the right (blue vectors) and left (red vectors) sides of the fish.

image points to target locations in the fluid. Alternating rows of calibration marks are offset in depth by 1 mm for calibration in the *z* direction (this offset is not visible in the Fig. 2A calibration images). Images of the target from each camera are analyzed, providing a pair of locations for each marker on the target: the *x*, *y* and *z* location of the marker point on the target in the fluid and its *x* and *y* pixel location in the image. A polynomial equation mapping function is created based on calibration grid points using a least-squares method; this equation is used to determine the spatial dimensions of the flow field. Use of the calibration grid and image mapping functions had the added advantage of aligning the images during processing so that the field of view of the cameras did not have to be aligned pixel to pixel. Areas seen by each individual camera that do not overlap the view from the other camera (approximately 15% of the field of view, Fig. 2A) are discarded prior to calculation of the three-dimensional vector field. Stereo-DPIV calibration and the required calculations are discussed extensively in the engineering literature (Gaydon et al., 1997; Lawson and Wu, 1997; Willert, 1997; Westerweel and van Oord, 2000) and will not be repeated here.

The first step in calculating the three-dimensional vector field is two-dimensional analysis of the simultaneously collected left and right images (Fig. 2B). Using Insight software (v. 3.3, TSI, Inc., USA), sequential pairs of video images (4 ms apart in time) were analyzed by subdividing the images into a series of interrogation areas and comparing pixel intensity in these areas using two-frame cross-correlation analysis. The areas of flow analyzed were typically rectangular in shape. The cross-correlation analysis used a Hart algorithm (Hart, 2000), a spot size of 64 pixels and a peak:noise ratio of 1.5. DPIV calculation methods have been previously described in detail (Willert and Gharib, 1991; Anderson, 1996; Raffel et al., 1998). The two components of velocity nominally perpendicular to the camera optical axis (in our case, *U* and *V)* are calculated from the two-dimensional recorded images (Fig. 2B). Note that the two-dimensional vectors are calculated in a symmetrical, aligned grid (Fig. 2B) based on the calibration grid (Fig. 2A).

The out-of-plane velocity component (in our case, *W*, Fig. 2C,D) is calculated using the two-dimensional vector files (Fig. 2B) and a set of four polynomial equations that determine the *W* component at each location in the two-dimensional vector fields. Interpolation of the right and left vector fields provides particle image displacements; fluid displacement is solved for using a least-squares method.

DPIV measurements

To visualize wake geometry, downstream free velocity (U_o) was subtracted from each three-dimensional velocity vector (see, for example, Fig. 3). Downstream rather than upstream velocity was subtracted because the presence of the fish affects the flow field. The method for subtracting U_o was based on the fact that the present visualizations showed defined, oscillating, posteriolaterally oriented jet flows in the trout wakes such as are associated with linked vortex ring wakes produced by body–caudal fin swimmers (e.g. Müller et al., 1997; Wolfgang et al., 1999; Drucker and Lauder, 2001b; Nauen and Lauder, 2002). In addition, previous studies of trout steady swimming kinematics (Stevens, 1979; Webb et al., 1984; Webb, 1988, 1993) and wake flow (Blickhan et al., 1992) indicate that the jet flows seen here are associated with a linked vortex-ring wake. The height of linked vortex-ring wakes produced during steady swimming is typically equal to caudal fin span (Blickhan et al., 1992; Müller et al., 2000; Nauen and Lauder, 2002). Thus, flow above and below the caudal fin represented free-stream velocity, and we evaluated free-stream velocity magnitudes in regions of the stereo-DPIV images above and below the caudal fin.

The magnitudes and directions of *U*, *V* and *W* were determined for 10 vectors in the central jet flow of the wake (Figs 2, 3) created by each stroke of the caudal fin. Six to eight consecutive strokes were analyzed for each individual. The ratio of the magnitudes of $U/(U+V+W)$, which is referred to hereafter as *U*/total wake flow, was calculated from the flow values. Froude propulsive efficiency (η_p) was also calculated as $2U_o(U-U_o)/(U^2+V^2+W^2-U_o^2)$ based on Blake (1983). Single-factor analyses of variance (ANOVAs) were performed

using SuperANOVA (version 1.11) to determine the effect of individual on the measured parameters, the ratio of *U*/total wake flow and η_p. All *F*-values were calculated as described by Zar (1984).

Results

During steady swimming at 1.2 *BL* s^{-1}, the wake of *Oncorhynchus mykiss* contained a directed jet of relatively high-velocity flow that alternated in direction to the left and right sides of the fish with the change in direction of the caudal fin at the end of each stroke (Figs 2C,D, 3). Stereo-DPIV methods produced three-dimensional views of the jets with their relatively high-velocity lateral flow components; the overlapping field of view area of approximately 90 cm^2 was characterized by more than 750 vectors (Fig. 3).

A series of jets was visible in the field of view of the cameras (e.g. Fig. 3B), which allows an evaluation of jet dynamics. The time-dependence of lateral (*W*) flows is depicted for an individual of 16.5 cm *BL* swimming at 1.2 *BL* s^{-1} (19.8 cm s^{-1}). A wake flow of approximately 6.6 cm in length, which was created over 0.33 s, is visible in a single image. Lateral flows are strong and consistent and showed defined directional reversals that resulted from the change in movement direction of the caudal fin with each stroke.

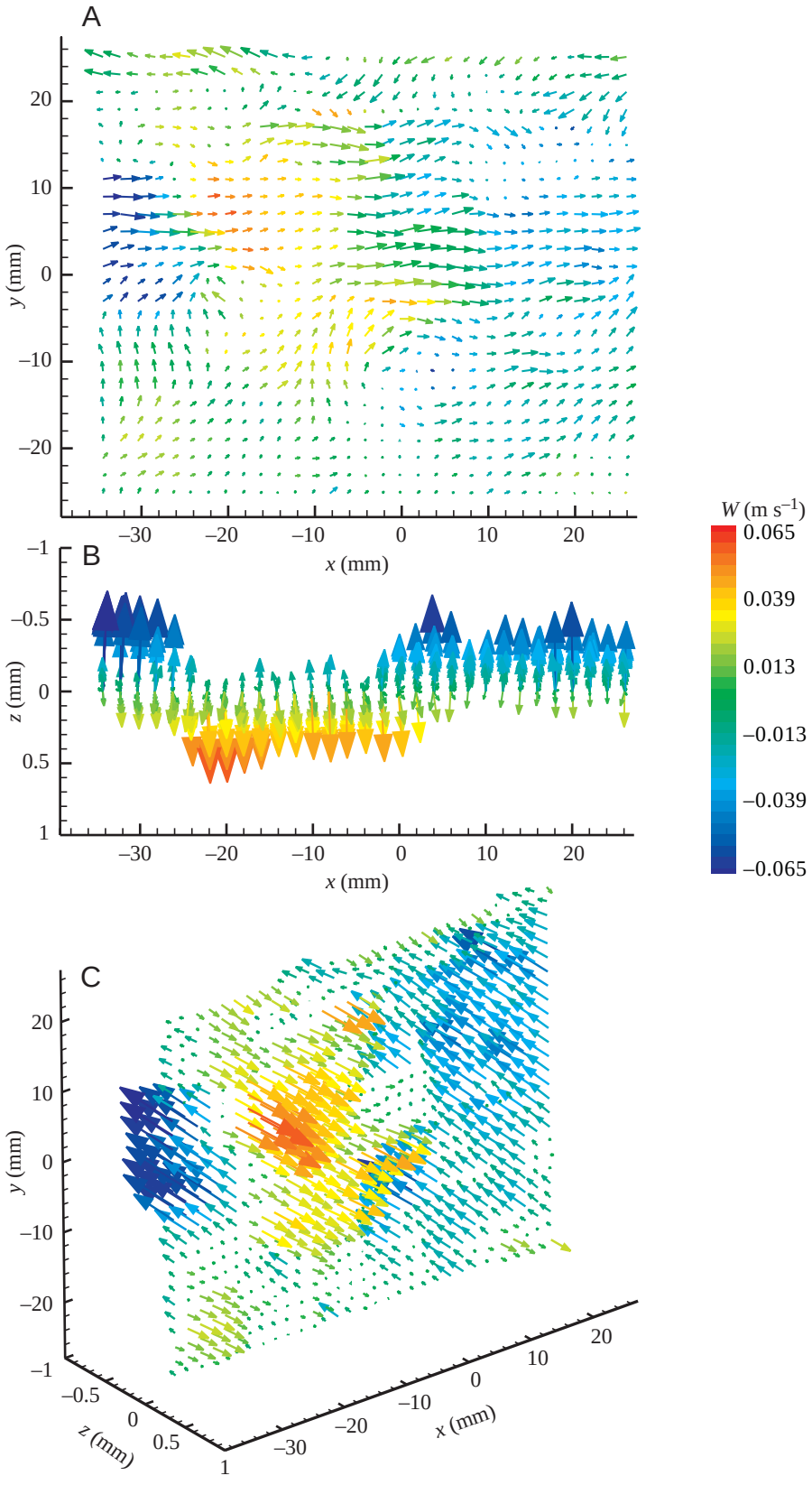

Fig. 3. Stereo-DPIV measurements of the wake of a 16.5 cm *BL* fish, where *BL* is total body length, swimming at 1.2 *BL* s^{-1} with free-stream flow subtracted to reveal wake structure. The caudal fin of the fish was positioned immediately upstream of the wake flow (i.e. to the left of the vector plot). Vector length indicates flow magnitude; vector color indicates the magnitude of *W* (m s^{-1}). The alternating areas of blue, red and blue vectors visible in the parasagittal plane (A) are clearly visible as regions of jet flow to the right and left of the fish, respectively, when viewed from above (B). Note that the lateral component of jet flow, emphasized here by the small scale of the *z*-axis for ease of viewing, is 10–60% greater in magnitude (on average) than that of *U* (see Fig. 4A). Rotating A counterclockwise also shows the alternating pattern of strong lateral jet flows. Ten vectors from the jet flow of 6–8 strokes for each individual were sampled to determine *U*, *V* and *W* magnitudes, where *U*, *V* and *W* are flow velocities in the downstream (*x*), vertical (*y*) and lateral (*z*) directions, respectively.

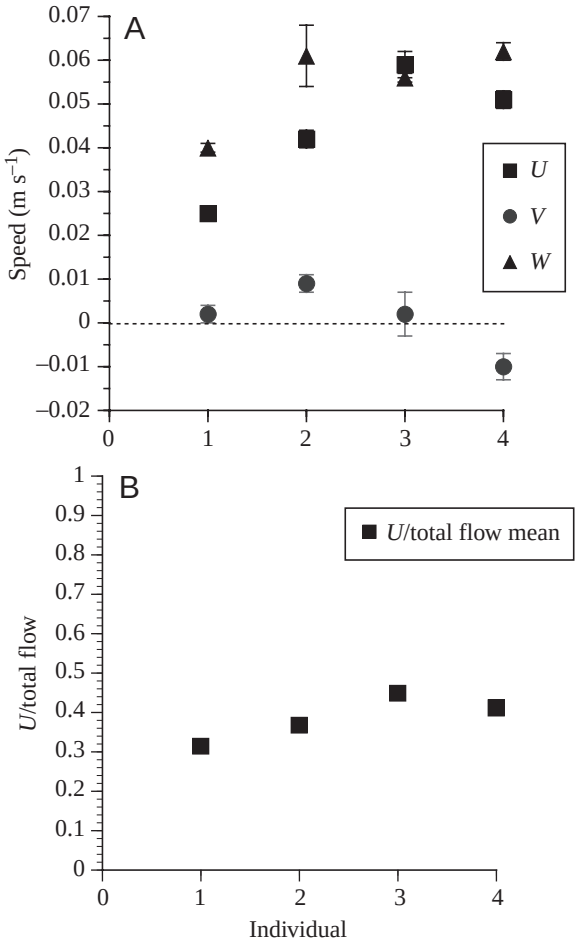

Fig. 4. The magnitudes (means ± S.E.M., *N*=60–80) of *U* and *W* wake flows, and the magnitude and direction (relative to the *x*-axis) of *V* flows as a function of individual (A). Ratio of *U*/total wake flow as a function of individual (B). Symbols represent means ± S.E.M. (error bars are smaller than the symbols), *N*=60–80. Freestream flow has been subtracted from *U*. *U*, *V* and *W* are flow velocities in the downstream (*x*), vertical (*y*) and lateral (*z*) directions, respectively.

Average vertical flows (*V*) were low in magnitude (typically less than 1 cm s^{-1}, Fig. 4A) and variable in direction (Fig. 4A). The magnitude and direction of *V* were dependent on individual (ANOVA, d.f.=3,286, *F*=6.9, *P*=0.0002). One individual (no. 2) typically produced small vertical flows in the upward direction (or positive flows, Fig. 4A). The other three individuals produced small vertical flows that were positive or negative (Fig. 4A) depending on the particular tail beat.

The magnitude of downstream flow (*U*) was also dependent on individual (ANOVA, d.f.=3,286, *F*=51.0, *P*=0.0001). *U* flows, of the order of 3–6 cm s^{-1} above free-stream velocity (Fig. 4A), were relatively substantial. Lateral flows (*W*), were typically the largest in magnitude, with average values of 4–6 cm s^{-1} (Fig. 4A), and were dependent on individual (ANOVA, d.f.=3,286, *F*=6.7, *P*=0.0002).

The ratio of *U*/total wake flow (a flow index of mechanical performance) was also dependent on individual (ANOVA, d.f.=3,286, *F*=15.6, *P*=0.0001). Mean *U*/total wake flow ratios for each individual (Fig. 4B) varied from 0.32±0.012 to 0.45±0.014 (mean ± S.E.M., *N*=60–80). Froude efficiency (η_p) was independent of individual (ANOVA, d.f.=3,286, *F*=1.67, *P*=0.17). On average, η_p was 0.74±0.01 (mean ± S.E.M., *N*=290).

Discussion

Stereo-DPIV

Stereo-DPIV is a unique method for the simultaneous calculation of *U*, *V* and *W* velocity components for flow fields created by free-swimming animals. In this case, the flow fields examined are wakes created by caudal fin locomotion by *Oncorhynchus mykiss*. Caudal fin wakes have been the subject of many studies using two-dimensional DPIV techniques (Stamhuis and Videler, 1995; Müller et al., 1997; Hanke et al., 2000; Lauder, 2000; Liao and Lauder, 2000; Müller et al., 2000, 2001; Drucker and Lauder, 2001b; Nauen and Lauder, 2002) but have not previously been visualized in three-dimensions. Characteristic of most of these wakes is the formation of linked vortex rings with laterally oriented central jet flow. Such jet flows were created during slow, steady, forward swimming by *O. mykiss* and were visible in high resolution (>750 vectors) using stereo-DPIV.

Previous studies have estimated three-dimensional wake geometry using two-dimensional DPIV methods (see, for example, Drucker and Lauder, 1999; Nauen and Lauder, 2002), which requires combining two-dimensional measurements made in at least two different planes (typically the parasagittal and frontal planes) measured during independent kinematic events. This combination of measurements requires study of a repetitive behavior with low kinematic variation. Such requirements are unnecessary with stereo-DPIV, however, as simultaneous calculation of *U*, *V* and *W* allows for three-dimensional visualization from measurements made using a single light sheet orientation. The 1–2 mm thickness of the light sheet used here limited the present *W* measurements to a subset of the total wake volume. Nevertheless, stereo-DPIV has high potential for three-dimensional flow visualization of non-repetitive, highly variable behaviors for which combining separate measurements from orthogonally oriented light sheets is not suitable.

Trout caudal fin locomotion

The swimming speed of 1.2 *BL* s^{-1} studied here has been used in previous studies of wake structure produced by caudal fin locomotion (Liao and Lauder, 2000; Drucker and Lauder, 2001b; Nauen and Lauder, 2002) and is close to speeds examined in other two-dimensional DPIV studies of caudal fin locomotion (Müller et al., 1997, 2001), which allows for direct comparison of the present wake structure data with wake structures described for other species. The data of Webb et al. (1984) indicate that the speed of 1.2 *BL* s^{-1} is well within the aerobic capacity limits of *O. mykiss*.

Stereo-DIPV revealed a strong, oscillating jet with a large

lateral flow component in the wake of *Oncorhynchus mykiss* swimming steadily at 1.2 *BL* s^{-1}. Such jets are typically associated with linked vortex ring wakes produced by body–caudal-fin locomotors (e.g. Müller et al., 1997; Wolfgang et al., 1999; Drucker and Lauder, 2001b; Nauen and Lauder, 2002). The magnitudes and directions of *U*, *V* and *W* flows in the wake correspond to the magnitude of reaction forces to the jet flow that powers locomotion. Of particular interest are the magnitude and direction of vertical flows produced by the caudal fin that may act to rotate the fish about its anteriorly positioned center of mass and the ratio of *U*/total wake flow, which is a flow index of caudal fin mechanical performance.

Vertical flows measured here were very small in magnitude and were variable in direction. *O. mykiss*, a member of the Salmoniformes, has a symmetrically shaped, or homocercal, forked caudal fin. It is traditionally assumed that caudal fins of this shape move symmetrically and generate forces in the horizontal plane only (for a review, see Lauder, 2000). The present data, and study of more derived teleosts with forked homocercal caudal fins, do not, however, support this assumption. During relatively slow, steady swimming, the caudal fin of bluegill sunfish *Lepomis macrochirus* tilts relative to the vertical (probably because of intrinsic tail muscle activity; Lauder, 2000) and produces ventrally inclined flows (Lauder, 2000). The homocercal forked caudal fin of chub mackerel *Scomber japonicus* also tilts relative to vertical during steady swimming (Gibb et al., 1999) and produces ventrally inclined flows and thus lift forces that tend to lower the head (Nauen and Lauder, 2002).

Vertical flows produced by homocercal caudal fins tend to be small in magnitude. For example, vertical forces are less than 3% of the total force production of slightly larger mackerel (23±1 cm fork length, mean ± S.E.M., *N*=4) swimming at 1.2 and 2.2 fork lengths s^{-1} (Nauen and Lauder, 2002). The low-magnitude *V* flows measured in the present study are thus similar to those for the more derived species (Lauder, 2000; Nauen and Lauder, 2002). The present data indicate, however, that, unlike *L. macrochirus* (Lauder, 2000) and *S. japonicus* (Nauen and Lauder, 2002), *O. mykiss* shows variable caudal fin vertical orientations during slow steady swimming. Indeed, on average, the flows produced by three out of the four individuals studied here were directed slightly upwards. This indicates the production of a lift force that would tend to raise the head, which is the opposite of previous findings.

There is also typically a strong lateral component to jet flow produced by caudal fin locomotion (Stamhuis and Videler, 1995; Müller et al., 1997; Hanke et al., 2000; Lauder, 2000; Liao and Lauder, 2000; Müller et al., 2000, 2001; Drucker and Lauder, 2001b; Nauen and Lauder, 2002), which signifies relatively strong lateral force production. Studies of both bluegill sunfish (Drucker and Lauder, 2001b) and chub mackerel (Nauen and Lauder, 2002) indicated that for animals swimming freely at a speed of approximately 1 *BL* s^{-1}, lateral forces are approximately twice the magnitude of thrust forces. *W* flows seen in the present study were typically greater in magnitude than *U*, although by a factor of less than two (Fig. 4).

High-magnitude *W* relative to *U* (and low-magnitude *V*) resulted in *U*/total wake flow ratios in the range 0.32–0.45. This ratio is a flow-based estimate of true mechanical performance (which is the ratio of thrust/total force). Mechanical performance ratios of the order of 0.3–0.4 have been determined using two-dimensional DPIV for caudal fin locomotion by slightly larger (approximately 23 cm *BL*) bluegill sunfish (Drucker and Lauder, 2001b) and chub mackerel (Nauen and Lauder, 2002) swimming at approximately 1 *BL* s^{-1}. These values are consistent with the present three-dimensional DPIV data for *O. mykiss*. Thus, data collected using two methods, from three distantly related euteleost taxa with a variety of body and fin shapes and a range of swimming performance capacities, indicate a high lateral force component during slow, steady caudal fin locomotion. It is possible that the relatively low mechanical performance of these taxa reflects an inherent limitation to caudal fin propulsion as a posteriorly propagated wave of lateral bending. Supporting this hypothesis is the finding of Triantafyllou et al. (1991) of optimum mechanical performance values of 0.2 for a foil oscillating transversely through uniform incoming flow (which is a physical model of caudal fin locomotion).

In contrast to these caudal fin mechanical performance values, our calculated mean Froude propulsive efficiency (η_p) of 0.74 was relatively high. The η_p value of 0.74 determined here for the single relative speed of 1.2 *BL* s^{-1} is somewhat larger than values determined previously using kinematic data. For example, Webb (1971a) calculated a η_p value of 0.54 using larger trout (30 cm *BL*) than those studied here swimming at speeds of approximately 1.25 *BL* s^{-1}. Values of η_p approached 0.7 as swimming speed increased to approximately 1.7–1.9 *BL* s^{-1} (see Table 11 in Webb, 1971a). In that study, η_p was calculated as the ratio of fish swimming speed to the speed of the body propulsive wave, on the basis that this is the ratio between the momentum added to the water by the propulsive wave and the amount of kinetic energy necessary to accelerate that water (Webb, 1971b). A later study (Webb et al., 1984) confirmed the conclusion that η_p increases with increasing speed for *O. mykiss*. An efficiency value of 0.7 was, however, previously determined for *O. mykiss* on the basis of power measurements calculated from automatic particle tracking and laser-Doppler anemometry techniques (Blickhan et al., 1992); however, few data and methodology details from that study are available for direct comparison with the present study.

The above range of η_p values suggests a relatively high propulsive efficiency for *O. mykiss* at slow cruising speeds, in contrast to the caudal fin mechanical performance values of 0.32–0.45. The η_p ratio reflects whole-body propulsive efficiency, including, for example, the volume of water accelerated by the fish (see the discussion in Blake, 1983), whereas caudal fin mechanical performance simply reflects the proportion of wake flow that is thrust. The finding that η_p is much greater than caudal fin mechanical performance suggests the involvement of additional factors (such as body shape and

propulsive wave amplitude and frequency), which might result in relatively high overall propulsive efficiencies even though the performance of any given propulsor is relatively low.

The use of stereo-DPIV to determine simultaneously all three velocity components allowed for calculations of both η_p and caudal fin mechanical efficiency for single kinematic events in the present study (rather than averaging over multiple events as is necessary with two-dimensional DPIV, Drucker and Lauder, 1999, 2000; Nauen and Lauder, 2002). The homocercal caudal fin shows flexibility in performance during steady forward locomotion with increasing speed, particularly in regard to vertical force production and increases in thrust/total force production as a function of speed (Nauen and Lauder, 2002). Future studies of the homocercal caudal fin of teleost fishes under a wider range of hydrodynamic conditions (including unsteady and maneuvering locomotion) are necessary to ascertain the extent of functional versatility in the caudal fins of different taxa. Including calculations of both η_p and caudal fin mechanical performance will allow a better understanding of the interplay between caudal fin performance and locomotor efficiency.

The authors thank Laura Farrell for assistance with obtaining trout and conducting the experiments. We also thank Laura Farrell, Ellen Freund, Tonia Hsieh, Jimmy Liao and especially Eric Tytell for helpful comments during the course of the study. Comments from two anonymous reviewers improved the manuscript. Support was provided by NSF grant IBN-9807012 to G.V.L.

References

Anderson, J. M. (1996). Vorticity control for efficient propulsion. PhD thesis, Massachusetts Institute of Technology and the Woods Hole Oceanographic Institution.

Blake, R. W. (1983). *Fish Locomotion*. New York: Cambridge University Press.

Blickhan, R., Krick, C., Zehren, D. and Nachtigall, W. (1992). Generation of a vortex chain in the wake of a subundulatory swimmer. *Naturwissenschaften* **79**, 220-221.

Coughlin, D. J. (2000). Power production during steady swimming in largemouth bass and rainbow trout. *J. Exp. Biol.* **203**, 617-629.

Drucker, E. G. and Lauder, G. V. (1999). Locomotor forces on a swimming fish: three-dimensional vortex wake dynamics quantified using digital particle image velocimetry. *J. Exp. Biol.* **202**, 2393-2412.

Drucker, E. G. and Lauder, G. V. (2000). A hydrodynamic analysis of fish swimming speed: wake structure and locomotory force in slow and fast labriform swimmers. *J. Exp. Biol.* **203**, 2379-2393.

Drucker, E. G. and Lauder, G. V. (2001a). Wake dynamics and fluid forces of turning maneuvers in sunfish. *J. Exp. Biol.* **204**, 431-442.

Drucker, E. G. and Lauder, G. V. (2001b). Locomotor function of the dorsal fin in teleost fishes: experimental analysis of wake forces in sunfish. *J. Exp. Biol.* **204**, 2943-2958.

Gaydon, M., Raffel, M., Willert, C., Rosengarten, M. and Kompenhans, J. (1997). Hydbrid stereoscopic particle image velocimetry. *Exp. Fluids* **23**, 331-334.

Gibb, A. C., Dickson, K. A. and Lauder, G. V. (1999). Tail kinematics of the chub mackerel *Scomber japonicus*: testing the homocercal tail model of fish propulsion. *J. Exp. Biol.* **202**, 2433-2447.

Hammond, L., Altringham, J. D. and Wardle, C. S. (1998). Myotomal slow muscle function of rainbow trout *Oncorhynchus mykiss* during steady swimming. *J. Exp. Biol.* **201**, 1659-1671.

Hanke, W., Brucker, C. and Bleckmann, H. (2000). The ageing of the low-frequency water disturbances caused by swimming goldfish and its possible relevance to prey detection. *J. Exp. Biol.* **203**, 1193-1200.

Hart, D. P. (2000). Super-resolution PIV by recursive local-correlation. *J. Vis.* **3**, 187-194.

Jayne, B. C., Lozada, A. F. and Lauder, G. V. (1996). Function of the dorsal fin in bluegill sunfish: motor patterns during four distinct locomotor behaviors. *J. Morphol.* **228**, 307-326.

Lauder, G. V. (2000). Function of the caudal fin during locomotion in fishes: kinematics, flow visualization, and evolutionary patterns. *Am. Zool.* **40**, 101-122.

Lawson, N. J. and Wu, J. (1997). Three-dimensional particle image velocimetry: experimental error analysis of a digital angular stereoscopic system. *Meas. Sci. Tech.* **8**, 1455-1464.

Liao, J. and Lauder, G. V. (2000). Function of the heterocercal tail in white sturgeon: flow visualization during steady swimming and vertical maneuvering. *J. Exp. Biol.* **203**, 3585-3594.

Müller, U. K., Smit, J., Stamhuis, E. J. and Videler, J. J. (2001). How the body contributes to the wake in undulatory fish swimming: flow fields of a swimming eel (*Anguilla anguilla*). *J. Exp. Biol.* **204**, 2751-2762.

Müller, U. K., Stamhuis, E. J. and Videler, J. J. (2000). Hydrodynamics of unsteady fish swimming and the effects of body size: comparing the flow fields of fish larvae and adults. *J. Exp. Biol.* **203**, 193-206.

Müller, U. K., Van Den Heuvel, B. L. E., Stamhuis, E. J. and Videler, J. J. (1997). Fish foot prints: morphology and energetics of the wake behind a continuously swimming mullet (*Chelon labrosus* Risso). *J. Exp. Biol.* **200**, 2893-2906.

Nauen, J. C. and Lauder, G. V. (2001). Locomotion in scombrid fishes: visualization of flow around the caudal peduncle and finlets of the chub mackerel *Scomber japonicus*. *J. Exp. Biol.* **204**, 2251-2263.

Nauen, J. C. and Lauder, G. V. (2002). Hydrodynamics of caudal fin locomotion by chub mackerel, *Scomber japonicus*. *J. Exp. Biol.* **205**, 1709-1724.

Raffel, M., Willert, C. and Kompenhans, J. (1998). *Particle Image Velocimetry: A Practical Guide*. New York: Springer.

Stamhuis, E. J. and Videler, J. J. (1995). Quantitative flow analysis around aquatic animals using laser sheet particle image velocimetry. *J. Exp. Biol.* **198**, 283-294.

Stevens, E. D. (1979). The effect of temperature on tail beat frequency of fish swimming at constant velocity. *Can. J. Zool.* **57**, 1628-1635.

Triantafyllou, M. S., Triantafyllou, G. S. and Gopalkrishnan, R. (1991). Wake mechanics for thrust generation in oscillating foils. *Phys. Fluids A* **3**, 2835-2837.

Videler, J. J., Müller, U. K. and Stamhuis, E. J. (1999). Aquatic vertebrate locomotion: wakes from body waves. *J. Exp. Biol.* **202**, 3423-3430.

Webb, P. W. (1971a). The swimming energetics of trout. I. Thrust and power output at cruising speeds. *J. Exp. Biol.* **55**, 489-520.

Webb, P. W. (1971b). The swimming energetics of trout. II. Oxygen consumption and swimming efficiency. *J. Exp. Biol.* **55**, 521-540.

Webb, P. W. (1988). 'Steady' swimming kinematics of tiger musky, an esociform accelerator, and rainbow trout, a generalist cruiser. *J. Exp. Biol.* **1988**, 51-69.

Webb, P. W. (1993). The effect of solid and porous channel walls on steady swimming of the steelhead trout *Oncorhynchus mykiss*. *J. Exp. Biol.* **178**, 97-108.

Webb, P. W., Kostecki, P. T. and Stevens, E. D. (1984). The effect of size and swimming speed on locomotor kinematics of rainbow trout. *J. Exp. Biol.* **109**, 77-95.

Westerweel, J. and von Oord, J. (2000). Stereoscopic PIV measurements in a turbulent boundary layer. In *Particle Image Velocimetry. Progress Towards Industrial Application* (ed. M. Stanislas, J. Kompenhans and J. Westerweel), pp. 459-478. Dordrecht: Kluwer Academic.

Wilga, C. D. and Lauder, G. V. (2000). Three-dimensional kinematics and wake structure of the pectoral fins during locomotion in leopard sharks *Triakis semifasciata*. *J. Exp. Biol.* **203**, 2261-2278.

Willert, C. (1997). Stereoscopic digital particle image velocimetry for application in wind tunnel flows. *Meas. Sci. Tech.* **8**, 1465-1479.

Willert, C. E. and Gharib, M. (1991). Digital particle image velocimetry. *Exp. Fluids* **10**, 181-193.

Wolfgang, M. J., Anderson, J. M., Grosenbaugh, M. A., Yue, D. K. P. and Triantafyllou, M. S. (1999). Near-body flow dynamics in swimming fish. *J. Exp. Biol.* **202**, 2303-2327.

Zar, J. H. (1984). *Biostatistical Analysis*. Englewood Cliffs: Prentice Hall.